An Adaptive Observer for Recirculation-Based Solid Oxide Fuel Cells

Singith Abeysiriwardena[1]
Mechanical and Aerospace
Engineering Department,
University of Central Florida,
Orlando, FL 32816
e-mail: singith.abeysiriwardena@knights.ucf.edu

Tuhin Das
Mechanical and Aerospace
Engineering Department,
University of Central Florida,
Orlando, FL 32816

In this paper, we present an observer design for online estimation of species concentrations in recirculation-based solid oxide fuel cell (SOFC) systems with integrated reformers. For the system considered, on-board reforming of methane results in mixture of several species of different concentrations along the fuel path. The presence of a fuel reformer gives way to coupling of system equations, in turn, increasing species interactions and complexity of the state equations. The knowledge of concentration of species at key locations in the fuel cell can help prevent cell damage and improve longevity. In this regard, the use of sensors to determine species concentration is an invasive process which is expensive to both utilize and maintain. While existing observers are designed either for chemical reactors or for a fuel cell exclusively, the proposed strategy aims to improve on that by considering a combined reformer and fuel cell and designing a nonlinear adaptive observer using readily measured concentrations and selected variables. For estimating certain critical indicators, such as fuel utilization, state transformations have been used in the design to obtain a more versatile and computationally efficient reduced order observer. The study develops detailed stability analysis of the observers and quantifies the effect of uncertainties on observer performance.
[DOI: 10.1115/1.4033271]

1 Introduction

In recent years, SOFC have attracted interests due to factors such as their fuel flexibility and tolerance to impurities. High-temperature operating conditions (800–1000 °C) of SOFCs are conducive to internal reforming of fuels, and the exhaust gases are excellent means for sustaining on-board fuel reforming. SOFCs are not only tolerant to carbon monoxide but can also use it as fuel. Furthermore, high operating temperatures makes SOFC-gas turbine hybrids excellent combined heat and power (CHP) systems. Optimal performance of SOFC systems can be realized through well-designed control strategies. Critical performance variables such as fuel utilization and steam-to-carbon ratio (STCR) play important roles in determining the overall efficiency and longevity of the system [1,2]. Hence, they must be controlled within safety limits during operation.

Utilization and STCR are functions of species concentrations. Hence, for implementing control algorithms, it is necessary to measure the concentrations. The reforming process in SOFCs results in a number of gaseous species in the reformer and the fuel cell. For instance, steam reforming of methane results in five species, namely, CH_4, CO, CO_2, H_2, and H_2O. Control of utilization and STCR would, therefore, require a large number of concentration sensors which would elevate costs and complicate the hardware. A means of reducing concentration sensors is to design observers that dynamically estimate the species concentrations. In this paper, we design an observer for a steam reformer-based tubular SOFC system with anode recirculation and methane as fuel. We develop a lumped control-oriented model that captures the details of heat and mass transfer, chemical kinetics, and electrochemical phenomena of the system. Our control-oriented model has similarities with the tubular SOFC models developed in Refs. [1] and [3]. The kinetics of steam reforming are modeled based on the experimental results in Ref. [4]. Other tubular SOFC system models appear in Refs. [5–8], and models of planar SOFC systems appear in Ref. [9] and references therein.

In the literature, there are few observer designs for fuel cell systems [10]; however, there exist estimation and adaptive control designs that focus exclusively on either chemical reactors or bioreactors [11]. In contrast, we consider a coupled steam reformer and fuel cell system. The observers in Refs. [12] and [13] rely on temperature dynamics. In our observer design, we refrain from using the temperature dynamics of the SOFC system. This is because high-temperature operating conditions can result in significant heat exchange through radiative means or otherwise, which would remain unmodeled. Several designs, such as Refs. [13] and [14], assume prior knowledge of reaction rates. However, in Ref. [15], the author shows estimation errors arising from uncertain reaction rate parameters and adopts an adaptive approach to circumvent this issue. In Ref. [12], the observer design is based on coordinate transformations that eliminate reaction rate terms. In our adaptive design, we treat the rates of steam reforming reactions as unknown parameters that must be dynamically estimated. In Ref. [10], the authors have designed an adaptive observer for hydrogen estimation in a polymer electrolyte membrane fuel cell. The observer considers the inlet hydrogen partial pressure as a slowly varying unknown parameter and uses voltage measurements. Using a linearized model for estimation of species concentration in a recirculation-based SOFC which is nonlinear by nature is difficult and cumbersome because too many operating points are needed. Hence, we propose a nonlinear observer design with minimal concentration sensors used along with cell voltage measurement. Furthermore, a reduced order observer using bulk flow rate sensors is developed if the focus will be on fuel utilization. The higher-order observer with some species concentration sensors and cell voltage measurement can be used if more insight into species concentration is needed.

This paper is organized as follows: In the Secs. 2 and 3, we describe the SOFC system and provide an outline of the system

[1]Corresponding author.

Contributed by the Dynamic Systems Division of ASME for publication in the Journal of Dynamic Systems, Measurement, and Control. Manuscript received June 30, 2015; final manuscript received March 25, 2016; published online May 25, 2016. Assoc. Editor: Ardalan Vahidi.

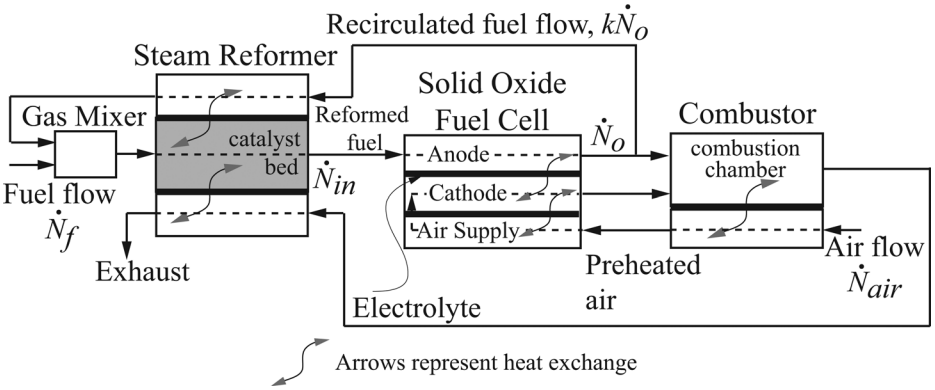

Fig. 1 Schematic diagram of the SOFC system

model. In our discussion on the SOFC model development, we first describe the SOFC system. In Sec. 3, we develop the mathematical model of the SOFC system. We first present the equations for the fundamental gas and solid control volume models. Sections 3.1 and 3.2 describe the steam reformer and SOFC system models. We focus primarily on the mass transfer phenomena and chemical kinetics. Although not elaborated in our discussion, the heat transfer phenomena of the system is modeled in detail but omitted here for the sake of brevity. Next, we present the problem and summarize our prior results. We then present the proposed dynamic observer design that uses cell voltage measurements. A reduced order observer for estimation of fuel utilization is subsequently developed. We prove the boundedness and convergence properties of the proposed observers followed by simulation results. Finally, we provide the concluding remarks.

2 System Overview

Our analysis is based on a steam reformer-based tubular SOFC system. The system consists of three primary components, namely, the steam reformer that produces a hydrogen-rich gas from a mixture of methane and steam, the SOFC that generates electricity from electrochemical reactions, and the combustor where excess fuel is burnt to generate heat. Methane is chosen as the fuel for the system, with a molar flow rate of $\dot{N}_f$. It is noted here that the analysis and control development approach can be extended to other fuels as well, such as methanol, ethanol, etc. The SOFC system is described in Fig. 1.

The reformer produces a hydrogen-rich gas which is supplied to the anode of the fuel cell. Electrochemical reactions occurring at the anode due to current draw result in a steam-rich gas mixture at the anode exit. A fraction k of the anode efflux is recirculated through the reformer into a mixing chamber where fuel is added. The recirculation k is assumed to a fixed known fraction. In tubular SOFCs, recirculation is typically achieved through the deliberate use of imperfect seals. The mixing of the two fluid streams and pressurization is achieved in the gas mixer using an ejector or a recirculating fuel pump, Ref. [2]. The steam reforming process occurring in the reformer catalyst bed is an endothermic process. The energy required to sustain the process is supplied from two sources, namely, the combustor efflux that is passed through the reformer and the aforementioned recirculated anode flow, as shown in Fig. 1. The remaining anode efflux is mixed with the cathode efflux in the combustion chamber. The combustor also serves to preheat the cathode air which has a molar flow rate of $\dot{N}_{\text{air}}$. The tubular construction of each cell causes the air to first enter the cell through the air supply tube and then reverse its direction to enter the cathode chamber. The cathode air serves as the source of oxygen for the fuel cell.

3 System Model

The essential dynamics of the SOFC system in Fig. 1 are modeled using fundamental solid volume and gas control volume models. The control development presented in this paper is primarily based on mass balance equations of the reformer and the fuel cell. Details of the model development as used for simulations are available in Ref. [16].

The mass balance equation for individual species is constructed as follows:

$$N_g\dot{\mathcal{X}}_{j,g} = \dot{\zeta}_{\text{in}}\mathcal{X}_{j,\text{in}} - \dot{\zeta}_{\text{ex}}\mathcal{X}_{j,g} + \mathcal{R}_{j,g}, \quad j = 1, 2, \ldots, 7 \tag{1}$$

where specific values of subscripts j, $j = 1, 2,\ldots,7$, correspond to the species CH_4, CO, CO_2, H_2, H_2O, N_2, and O_2, respectively. From Eq. (1) exploiting conservation of mass when all species are considered, we additionally have

$$\sum_{j=1}^{7}\mathcal{X}_{j,\text{in}} = \sum_{j=1}^{7}\mathcal{X}_{j,g} = 1 \Rightarrow \sum_{j=1}^{7}\dot{\mathcal{X}}_{j,g} = 0 \Rightarrow \dot{\zeta}_{\text{ex}} = \dot{\zeta}_{\text{in}} + \sum_{j=1}^{7}\mathcal{R}_{j,g} \tag{2}$$

3.1 Reformer Model. For steam reforming of methane we consider a packed-bed tubular reformer with nickel–alumina catalyst [17]. A schematic diagram of the steam reformer is shown in Fig. 2. The exhaust, reformate, and recirculated flows are modeled using gas control volumes and the catalyst bed is modeled as a solid volume. The details of heat transfer characteristics of the system are given in Ref. [1] and are not repeated here. Instead, we emphasize on the reformer reaction kinetics and mass transfer phenomena. The three main reactions that simultaneously occur during steam reforming of methane are [4]

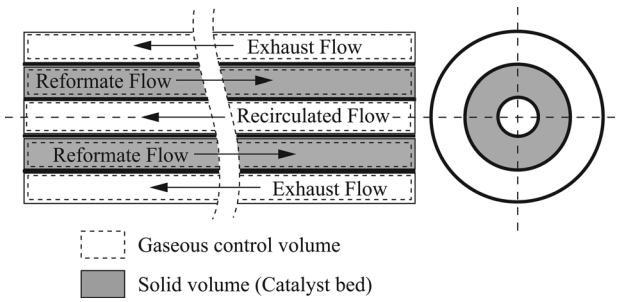

Fig. 2 Schematic diagram of tubular steam reformer

$$\begin{aligned}&\text{(I)} && CH_4 + H_2O \leftrightarrow CO + 3H_2\\ &\text{(II)} && CO + H_2O \leftrightarrow CO_2 + H_2\\ &\text{(III)} && CH_4 + 2H_2O \leftrightarrow CO_2 + 4H_2\end{aligned} \tag{3}$$

From Fig. 1, the mass balance equations for CH_4, CO, CO_2, H_2, and H_2O can be written using Eq. (1) as follows:

$$\begin{aligned}N_r\dot{\mathcal{X}}_{1,r} &= k\dot{N}_o\mathcal{X}_{1,a} - \dot{N}_{\text{in}}\mathcal{X}_{1,r} + \mathcal{R}_{1,r} + \dot{N}_f\\ N_r\dot{\mathcal{X}}_{2,r} &= k\dot{N}_o\mathcal{X}_{2,a} - \dot{N}_{\text{in}}\mathcal{X}_{2,r} + \mathcal{R}_{2,r}\\ N_r\dot{\mathcal{X}}_{3,r} &= k\dot{N}_o\mathcal{X}_{3,a} - \dot{N}_{\text{in}}\mathcal{X}_{3,r} + \mathcal{R}_{3,r}\\ N_r\dot{\mathcal{X}}_{4,r} &= k\dot{N}_o\mathcal{X}_{4,a} - \dot{N}_{\text{in}}\mathcal{X}_{4,r} + \mathcal{R}_{4,r}\\ N_r\dot{\mathcal{X}}_{5,r} &= k\dot{N}_o\mathcal{X}_{5,a} - \dot{N}_{\text{in}}\mathcal{X}_{5,r} + \mathcal{R}_{5,r}\end{aligned} \tag{4}$$

where $N_r = P_rV_r/R_uT_r$ and k is the anode recirculation fraction, as indicated in Fig. 1. Note that the reformer inlet and exit flows shown in Fig. 1 do not contain O_2 and N_2. Hence, $\mathcal{X}_{6,r} = \mathcal{X}_{7,r} = 0$ and $\mathcal{R}_{6,r} = \mathcal{R}_{7,r} = 0$. From Eq. (3), we express $\mathcal{R}_{j,r}$, $j = 1, 2, \ldots, 5$ in terms of the reaction rates r_{I}, r_{II}, and r_{III} as follows:

$$\mathbf{R}_r = \mathbf{G}\,\mathbf{r}, \mathbf{G} = \begin{bmatrix}-1 & 0 & -1\\ 1 & -1 & 0\\ 0 & 1 & 1\\ 3 & 1 & 4\\ -1 & -1 & -2\end{bmatrix}, \quad \mathbf{R}_r = \begin{bmatrix}\mathcal{R}_{1,r}\\ \mathcal{R}_{2,r}\\ \mathcal{R}_{3,r}\\ \mathcal{R}_{4,r}\\ \mathcal{R}_{5,r}\end{bmatrix} \tag{5}$$

$\mathbf{r} = [r_{\text{I}}, r_{\text{II}}, r_{\text{III}}]^{\text{T}}$. Since $\mathbf{G}$ has a rank of 2, therefore, there are only two independent reaction rates among $\mathcal{R}_{j,r}$, $j = 1, 2, \ldots, 5$. Considering the rate of formation of CH_4 and CO in the reformer to be independent, we can write

$$\begin{aligned}\mathcal{R}_{3,r} &= -\mathcal{R}_{1,r} - \mathcal{R}_{2,r}\\ \mathcal{R}_{4,r} &= -4\mathcal{R}_{1,r} - \mathcal{R}_{2,r}\\ \mathcal{R}_{5,r} &= 2\mathcal{R}_{1,r} + \mathcal{R}_{2,r}\end{aligned} \tag{6}$$

and rewrite Eq. (4) as follows:

$$\begin{aligned}N_r\dot{\mathcal{X}}_{1,r} &= k\dot{N}_o\mathcal{X}_{1,a} - \dot{N}_{\text{in}}\mathcal{X}_{1,r} + \mathcal{R}_{1,r} + \dot{N}_f\\ N_r\dot{\mathcal{X}}_{2,r} &= k\dot{N}_o\mathcal{X}_{2,a} - \dot{N}_{\text{in}}\mathcal{X}_{2,r} + \mathcal{R}_{2,r}\\ N_r\dot{\mathcal{X}}_{3,r} &= k\dot{N}_o\mathcal{X}_{3,a} - \dot{N}_{\text{in}}\mathcal{X}_{3,r} - \mathcal{R}_{1,r} - \mathcal{R}_{2,r}\\ N_r\dot{\mathcal{X}}_{4,r} &= k\dot{N}_o\mathcal{X}_{4,a} - \dot{N}_{\text{in}}\mathcal{X}_{4,r} - 4\mathcal{R}_{1,r} - \mathcal{R}_{2,r}\\ N_r\dot{\mathcal{X}}_{5,r} &= k\dot{N}_o\mathcal{X}_{5,a} - \dot{N}_{\text{in}}\mathcal{X}_{5,r} + 2\mathcal{R}_{1,r} + \mathcal{R}_{2,r}\end{aligned} \tag{7}$$

From Eqs. (2) and (7) we deduce

$$\dot{N}_{\text{in}} = k\dot{N}_o + \dot{N}_f + \sum_{j=1}^{7}\mathcal{R}_{j,r} \Rightarrow \dot{N}_{\text{in}} = k\dot{N}_o + \dot{N}_f - 2\mathcal{R}_{1,r} \tag{8}$$

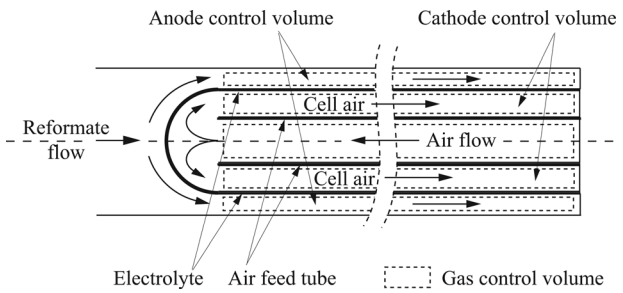

Fig. 3 Schematic diagram of tubular SOFC

3.2 SOFC Model. We assume our system to be comprised of $\mathcal{N}_{\text{cell}}$ tubular SOFC, connected in series. A schematic diagram of an individual cell is shown in Fig. 3. The anode, cathode, and air flows are modeled using gas control volumes. The air-feed tube and the electrolyte are modeled as solid volumes. The following chemical and electrochemical reactions occur simultaneously in the anode control volume:

$$\begin{aligned}&\text{(I)} && CH_4 + H_2O \leftrightarrow CO + 3H_2\\ &\text{(II)} && CO + H_2O \leftrightarrow CO_2 + H_2\\ &\text{(III)} && CH_4 + 2H_2O \leftrightarrow CO_2 + 4H_2\\ &\text{(IV)} && H_2 + O^{2-} \rightarrow H_2O + 2e\end{aligned} \tag{9}$$

Steam reforming, represented by reactions I, II, and III, occurs in the anode due to high temperatures and the presence of nickel catalyst. The primary electrochemical process is steam generation from H_2, described by reaction IV. Simultaneous electrochemical conversion of CO to CO_2 in the anode is also possible. However, this electrochemical reaction is ignored, since its reaction rate is much slower in presence of reactions II and IV, as indicated in Refs. [18] and references therein.

From Fig. 1 and Eq. (1), the mass balance equations for CH_4, CO, CO_2, H_2, and H_2O can be written as

$$\begin{aligned}N_a\dot{\mathcal{X}}_{1,a} &= -\dot{N}_o\mathcal{X}_{1,a} + \dot{N}_{\text{in}}\mathcal{X}_{1,r} + \mathcal{R}_{1,a}\\ N_a\dot{\mathcal{X}}_{2,a} &= -\dot{N}_o\mathcal{X}_{2,a} + \dot{N}_{\text{in}}\mathcal{X}_{2,r} + \mathcal{R}_{2,a}\\ N_a\dot{\mathcal{X}}_{3,a} &= -\dot{N}_o\mathcal{X}_{3,a} + \dot{N}_{\text{in}}\mathcal{X}_{3,r} + \mathcal{R}_{3,a}\\ N_a\dot{\mathcal{X}}_{4,a} &= -\dot{N}_o\mathcal{X}_{4,a} + \dot{N}_{\text{in}}\mathcal{X}_{4,r} + \mathcal{R}_{4,a} - r_e\\ N_a\dot{\mathcal{X}}_{5,a} &= -\dot{N}_o\mathcal{X}_{5,a} + \dot{N}_{\text{in}}\mathcal{X}_{5,r} + \mathcal{R}_{5,a} + r_e\end{aligned} \tag{10}$$

where $N_a = P_aV_a/R_uT_a$ and r_e is the rate of electrochemical reaction given by

$$r_e = \frac{i\mathcal{N}_{\text{cell}}}{nF} \tag{11}$$

Since current i can be measured, the rate of electrochemical reaction r_e is considered known. As with the reformate control volume, the anode inlet and exit flows do not contain O_2 and N_2. Therefore, $\mathcal{X}_{6,a} = \mathcal{X}_{7,a} = 0$. From Eq. (9), we express $\mathcal{R}_{j,a}$, $j = 1, 2, \ldots, 5$ in terms of the reaction rates r_{I}, r_{II}, and r_{III} as follows:

$$\mathbf{R}_a = \mathbf{G}\,\mathbf{r} + r_e[0\ \ 0\ \ 0 - 1\ \ 1]^{\text{T}}$$

where $\mathbf{R}_a = [\mathcal{R}_{1,a}\ \mathcal{R}_{2,a}\ \mathcal{R}_{3,a}\ \mathcal{R}_{4,a}\ \mathcal{R}_{5,a}]^{\text{T}}$, and $\mathbf{G}$ and $\mathbf{r}$ are given in Eq. (5). Since $\mathbf{G}$ has a rank of 2 and r_e is known, therefore, there are only two independent reaction rates among $\mathcal{R}_{j,a}$, $j = 1, 2, \ldots, 5$. Considering $\mathcal{R}_{1,a}$ and $\mathcal{R}_{2,a}$ to be independent, we can write

$$\begin{aligned}\mathcal{R}_{3,a} &= -\mathcal{R}_{1,a} - \mathcal{R}_{2,a}\\ \mathcal{R}_{4,a} &= -4\mathcal{R}_{1,a} - \mathcal{R}_{2,a} - r_e\\ \mathcal{R}_{5,a} &= 2\mathcal{R}_{1,a} + \mathcal{R}_{2,a} + r_e\end{aligned} \tag{12}$$

and rewrite Eq. (10) as

$$\begin{aligned}N_a\dot{\mathcal{X}}_{1,a} &= -\dot{N}_o\mathcal{X}_{1,a} + \dot{N}_{\text{in}}\mathcal{X}_{1,r} + \mathcal{R}_{1,a}\\ N_a\dot{\mathcal{X}}_{2,a} &= -\dot{N}_o\mathcal{X}_{2,a} + \dot{N}_{\text{in}}\mathcal{X}_{2,r} + \mathcal{R}_{2,a}\\ N_a\dot{\mathcal{X}}_{3,a} &= -\dot{N}_o\mathcal{X}_{3,a} + \dot{N}_{\text{in}}\mathcal{X}_{3,r} - \mathcal{R}_{1,a} - \mathcal{R}_{2,a}\\ N_a\dot{\mathcal{X}}_{4,a} &= -\dot{N}_o\mathcal{X}_{4,a} + \dot{N}_{\text{in}}\mathcal{X}_{4,r} - 4\mathcal{R}_{1,a} - \mathcal{R}_{2,a} - r_e\\ N_a\dot{\mathcal{X}}_{5,a} &= -\dot{N}_o\mathcal{X}_{5,a} + \dot{N}_{\text{in}}\mathcal{X}_{5,r} + 2\mathcal{R}_{1,a} + \mathcal{R}_{2,a} + r_e\end{aligned} \tag{13}$$

From Eqs. (2) and (13) we deduce that

$$\dot{N}_o = \dot{N}_{\text{in}} + \sum_{j=1}^{7} \mathcal{R}_{j,a} \Rightarrow \dot{N}_o = \dot{N}_{\text{in}} - 2\mathcal{R}_{1,a} \tag{14}$$

The electrochemical conversion of O_2 to O^{2-} ions takes place in the cathode control volume

$$\frac{1}{2}O_2 + 2e \rightarrow O^{2-} \tag{15}$$

with the reaction rate as given in Eq. (11). Considering the mole fractions of N_2 and O_2 in air to be 0.79 and 0.21, respectively, the mass balance equations of the cathode control volume can be written from Eqs. (11) and (15) as follows:

$$\begin{aligned} N_c\dot{\mathcal{X}}_{6,c} &= 0.79\dot{N}_{\text{air}} - \left(\dot{N}_{\text{air}} - \frac{r_{\text{IV}}}{2}\right)\mathcal{X}_{6,c} \\ N_c\dot{\mathcal{X}}_{7,c} &= 0.21\dot{N}_{\text{air}} - \left(\dot{N}_{\text{air}} - \frac{r_{\text{IV}}}{2}\right)\mathcal{X}_{7,c} - \frac{r_{\text{IV}}}{2} \\ \mathcal{X}_{i,c} &= 0, \quad i = 1, 2, \ldots, 5 \end{aligned} \tag{16}$$

4 Problem Statement and Prior Design

The observer design problem statement is as follows: given that temperatures and pressures can be sensed in the reformer and anode volumes, and given that the fuel cell current and voltage can be measured, design an observer for estimation of rates of steam reformation reactions, molar flow rates, and species concentrations using a minimum number of concentration sensors.

We summarize our prior observer design [19] which used four concentration sensors. The sensing requirement is that any two species of the gas mixture must be sensed at the reformer and anode exits. We state the equations for a sample observer design where CH_4 and CO concentrations are sensed in the reformer and anode volumes, i.e., measurements of $\mathcal{X}_{1,r}$, $\mathcal{X}_{1,a}$, $\mathcal{X}_{2,r}$, $\mathcal{X}_{2,a}$ are assumed to be available. Note that this choice is arbitrary and similar observers can be designed by sensing any two of CH_4, CO, CO_2, H_2, and H_2O at the reformer and anode exits. The variables to be estimated are $\dot{N}_{\text{in}}$, $\dot{N}_o$, $\mathcal{R}_{2,r}$, $\mathcal{R}_{2,a}$, $\mathcal{X}_{i,r}$, $\mathcal{X}_{i,a}$, $i = 1, 2, \ldots, 5$. Their estimates are denoted by $\hat{\dot{N}}_{\text{in}}$, $\hat{\dot{N}}_o$, $\hat{\mathcal{R}}_{2,r}$, $\hat{\mathcal{R}}_{2,a}$, $\hat{\mathcal{X}}_{i,r}$, $\hat{\mathcal{X}}_{i,a}$, $i = 1, 2, \ldots, 5$. Based on Eqs. (7), (8), (13), and (14), the following observer equations are proposed.

Using Eqs. (8) and (14) to express $\mathcal{R}_{1,r}$ and $\mathcal{R}_{1,a}$ in terms of the flow rates effectively reducing the order of the observer and using Eqs. (7) and (13), we get the structure of the observer equations as

$$\begin{aligned}
N_r\dot{\hat{\mathcal{X}}}_{1,r} &= k\hat{\dot{N}}_o(\hat{\mathcal{X}}_{1,a} + 0.5) - \hat{\dot{N}}_{\text{in}}(\hat{\mathcal{X}}_{1,r} + 0.5) + \mathcal{L}_{1,r}\,\mathcal{E}_{1,r} + 1.5\dot{N}_f \\
N_a\dot{\hat{\mathcal{X}}}_{1,a} &= -\hat{\dot{N}}_o(\hat{\mathcal{X}}_{1,a} + 0.5) + \hat{\dot{N}}_{\text{in}}(\hat{\mathcal{X}}_{1,r} + 0.5) + \mathcal{L}_{1,a}\,\mathcal{E}_{1,a} \\
N_r\dot{\hat{\mathcal{X}}}_{2,r} &= k\hat{\dot{N}}_o\hat{\mathcal{X}}_{2,a} - \hat{\dot{N}}_{\text{in}}\hat{\mathcal{X}}_{2,r} + \hat{\mathcal{R}}_{2,r} + \mathcal{L}_{2,r}\,\mathcal{E}_{2,r} \\
N_a\dot{\hat{\mathcal{X}}}_{2,a} &= -\hat{\dot{N}}_o\hat{\mathcal{X}}_{2,a} + \hat{\dot{N}}_{\text{in}}\hat{\mathcal{X}}_{2,r} + \hat{\mathcal{R}}_{2,a} + \mathcal{L}_{2,a}\,\mathcal{E}_{2,a} \\
N_r\dot{\hat{\mathcal{X}}}_{3,r} &= k\hat{\dot{N}}_o(\hat{\mathcal{X}}_{3,a} - 0.5) - \hat{\dot{N}}_{\text{in}}(\hat{\mathcal{X}}_{3,r} - 0.5) - 0.5\dot{N}_f - \hat{\mathcal{R}}_{2,r} \\
N_a\dot{\hat{\mathcal{X}}}_{3,a} &= -\hat{\dot{N}}_o(\hat{\mathcal{X}}_{3,a} - 0.5) + \hat{\dot{N}}_{\text{in}}(\hat{\mathcal{X}}_{3,r} - 0.5) - \hat{\mathcal{R}}_{2,a} \\
N_r\dot{\hat{\mathcal{X}}}_{4,r} &= k\hat{\dot{N}}_o(\hat{\mathcal{X}}_{4,a} - 2) - \hat{\dot{N}}_{\text{in}}(\hat{\mathcal{X}}_{4,r} - 2) - 2\dot{N}_f - \hat{\mathcal{R}}_{2,r} \\
N_a\dot{\hat{\mathcal{X}}}_{4,a} &= -\hat{\dot{N}}_o(\hat{\mathcal{X}}_{4,a} - 2) + \hat{\dot{N}}_{\text{in}}(\hat{\mathcal{X}}_{4,r} - 2) - \hat{\mathcal{R}}_{2,a} - i\mathcal{N}_{\text{cell}}/nF \\
N_r\dot{\hat{\mathcal{X}}}_{5,r} &= k\hat{\dot{N}}_o(\hat{\mathcal{X}}_{5,a} + 1) - \hat{\dot{N}}_{\text{in}}(\hat{\mathcal{X}}_{5,r} - 1) + \dot{N}_f + \hat{\mathcal{R}}_{2,r} \\
N_a\dot{\hat{\mathcal{X}}}_{5,a} &= -\hat{\dot{N}}_o(\hat{\mathcal{X}}_{5,a} + 1) + \hat{\dot{N}}_{\text{in}}(\hat{\mathcal{X}}_{5,r} + 1) + \hat{\mathcal{R}}_{2,a} + i\mathcal{N}_{\text{cell}}/nF
\end{aligned}$$

Since direct measurements of the slowly varying parameters $\dot{N}_{\text{in}}$, $\dot{N}_o$ and formation rates $\mathcal{R}_{2,r}$ and $\mathcal{R}_{2,a}$ are not available, the following adaptation laws were derived exploiting the fact that $\mathcal{X}_{1,r}$, $\mathcal{X}_{1,a}$, $\mathcal{X}_{2,r}$, and $\mathcal{X}_{2,a}$ are corelated to the above parameters:

$$\begin{aligned}
\dot{\hat{N}}_{\text{in}} &= \gamma_1[(\mathcal{E}_{1,a} - \mathcal{E}_{1,r})(\hat{\mathcal{X}}_{1,r} + 0.5) + (\mathcal{E}_{2,a} - \mathcal{E}_{2,r})\hat{\mathcal{X}}_{2,r}] \\
\dot{\hat{N}}_o &= \gamma_2[(k\mathcal{E}_{1,r} - \mathcal{E}_{1,a})(\hat{\mathcal{X}}_{1,a} + 0.5) + (k\mathcal{E}_{2,r} - \mathcal{E}_{2,a})\hat{\mathcal{X}}_{2,a}] \\
\dot{\hat{\mathcal{R}}}_{2,r} &= \gamma_3\,\mathcal{E}_{2,r} \\
\dot{\hat{\mathcal{R}}}_{2,a} &= \gamma_4\,\mathcal{E}_{2,a}
\end{aligned}$$

where $\gamma_1, \gamma_2, \gamma_3, \gamma_4 > 0$, $\mathcal{L}_{1,r}, \mathcal{L}_{1,a}, \mathcal{L}_{2,r}, \mathcal{L}_{2,a} > 0$, $\mathcal{E}_{1,r} = \mathcal{X}_{1,r} - \hat{\mathcal{X}}_{1,r}$, $\mathcal{E}_{1,a} = \mathcal{X}_{1,a} - \hat{\mathcal{X}}_{1,a}$, $\mathcal{E}_{2,r} = \mathcal{X}_{2,r} - \hat{\mathcal{X}}_{2,r}$, and $\mathcal{E}_{2,a} = \mathcal{X}_{2,a} - \hat{\mathcal{X}}_{2,a}$. This nonlinear observer guarantees uniform asymptotic stability of the observer error dynamics [19].

5 Design Using Cell Voltage Measurement

5.1 Observer Design. In Sec. 4, we have outlined an observer design procedure that uses four concentration sensors. In this section, we propose an observer design that uses cell voltage measurement and three concentration sensors, reducing the number of required concentration sensors by one. The three required concentration sensors are a steam and a hydrogen sensor at the reformer outlet and a steam sensor at the anode outlet. Hence, in addition to cell voltage V_{cell}, the measurements of $\mathcal{X}_{4,r}$, $\mathcal{X}_{5,r}$, and $\mathcal{X}_{5,a}$ are assumed to be available. The observer equations are

$$\begin{aligned}
N_r\dot{\hat{\mathcal{X}}}_{1,r} &= k\hat{\dot{N}}_o(\hat{\mathcal{X}}_{1,a} + 0.5) - \hat{\dot{N}}_{\text{in}}(\hat{\mathcal{X}}_{1,r} + 0.5) + 1.5\dot{N}_f + \eta_{1,r} \\
N_a\dot{\hat{\mathcal{X}}}_{1,a} &= -\hat{\dot{N}}_o(\hat{\mathcal{X}}_{1,a} + 0.5) + \hat{\dot{N}}_{\text{in}}(\hat{\mathcal{X}}_{1,r} + 0.5) + \eta_{1,a} \\
N_r\dot{\hat{\mathcal{X}}}_{2,r} &= k\hat{\dot{N}}_o\hat{\mathcal{X}}_{2,a} - \hat{\dot{N}}_{\text{in}}\hat{\mathcal{X}}_{2,r} + \hat{\mathcal{R}}_{2,r} + \eta_{2,r} \\
N_a\dot{\hat{\mathcal{X}}}_{2,a} &= -\hat{\dot{N}}_o\hat{\mathcal{X}}_{2,a} + \hat{\dot{N}}_{\text{in}}\hat{\mathcal{X}}_{2,r} + \hat{\mathcal{R}}_{2,a} + \eta_{2,a} \\
N_r\dot{\hat{\mathcal{X}}}_{3,r} &= k\hat{\dot{N}}_o(\hat{\mathcal{X}}_{3,a} - 0.5) - \hat{\dot{N}}_{\text{in}}(\hat{\mathcal{X}}_{3,r} - 0.5) - 0.5\dot{N}_f \\
&\quad - \hat{\mathcal{R}}_{2,r} + \eta_{3,r} \\
N_a\dot{\hat{\mathcal{X}}}_{3,a} &= -\hat{\dot{N}}_o(\hat{\mathcal{X}}_{3,a} - 0.5) + \hat{\dot{N}}_{\text{in}}(\hat{\mathcal{X}}_{3,r} - 0.5) - \hat{\mathcal{R}}_{2,a} + \eta_{3,a} \\
N_r\dot{\hat{\mathcal{X}}}_{4,r} &= k\hat{\dot{N}}_o(\hat{\mathcal{X}}_{4,a} - 2) - \hat{\dot{N}}_{\text{in}}(\hat{\mathcal{X}}_{4,r} - 2) - 2\dot{N}_f - \hat{\mathcal{R}}_{2,r} \\
&\quad + \mathcal{L}_{4,r}\,\mathcal{E}_{4,r} + \eta_{4,r} \\
N_a\dot{\hat{\mathcal{X}}}_{4,a} &= -\hat{\dot{N}}_o(\hat{\mathcal{X}}_{4,a} - 2) + \hat{\dot{N}}_{\text{in}}(\hat{\mathcal{X}}_{4,r} - 2) - \hat{\mathcal{R}}_{2,a} \\
&\quad - i\mathcal{N}_{\text{cell}}/nF + \eta_{4,a} \\
N_r\dot{\hat{\mathcal{X}}}_{5,r} &= k\hat{\dot{N}}_o(\hat{\mathcal{X}}_{5,a} + 1) - \hat{\dot{N}}_{\text{in}}(\hat{\mathcal{X}}_{5,r} + 1) + \dot{N}_f + \hat{\mathcal{R}}_{2,r} \\
&\quad + \mathcal{L}_{5,r}\,\mathcal{E}_{5,r} + \eta_{5,r} \\
N_a\dot{\hat{\mathcal{X}}}_{5,a} &= -\hat{\dot{N}}_o(\hat{\mathcal{X}}_{5,a} + 1) + \hat{\dot{N}}_{\text{in}}(\hat{\mathcal{X}}_{5,r} + 1) + \hat{\mathcal{R}}_{2,a} \\
&\quad + i\mathcal{N}_{\text{cell}}/nF + \mathcal{L}_{5,a}\,\mathcal{E}_{5,a} + \eta_{5,a}
\end{aligned} \tag{17}$$

with the following adaptation laws:

$$\begin{aligned}
\dot{\hat{N}}_{in} &= \gamma_1[(\mathcal{E}_{4,r}/N_r - \xi_{4,a}/N_a)(2 - \hat{\mathcal{X}}_{4,r}) \\
&\quad + (\mathcal{E}_{5,a}/N_a - \mathcal{E}_{5,r}/N_r)\,(\hat{\mathcal{X}}_{5,r} + 1)] + \eta_{p1} \\
\dot{\hat{N}}_o &= \gamma_2[(k\mathcal{E}_{4,r}/N_r - \xi_{4,a}/N_a)(\hat{\mathcal{X}}_{4,a} - 2) \\
&\quad + (k\mathcal{E}_{5,r}/N_r - \mathcal{E}_{5,a}/N_a)\,(\hat{\mathcal{X}}_{5,a} + 1)] + \eta_{p2} \\
\dot{\hat{\mathcal{R}}}_{2,r} &= \gamma_3\,[\mathcal{E}_{5,r}/N_r - \mathcal{E}_{4,r}/N_r] + \eta_{p3} \\
\dot{\hat{\mathcal{R}}}_{2,a} &= \gamma_4\,[\mathcal{E}_{5,a}/N_a - \xi_{4,a}/N_a] + \eta_{p4}
\end{aligned} \tag{18}$$

where

$$\mathcal{E}_{4,r} = \mathcal{X}_{4,r} - \hat{\mathcal{X}}_{4,r}, \quad \mathcal{E}_{5,r} = \mathcal{X}_{5,r} - \hat{\mathcal{X}}_{5,r}, \quad \mathcal{E}_{5,a} = \mathcal{X}_{5,a} - \hat{\mathcal{X}}_{5,a} \tag{19}$$

and $\mathcal{L}_{4,r}$, $\mathcal{L}_{5,r}$, $\mathcal{L}_{5,a}$, γ_1, γ_2, γ_3, and γ_4 are positive constants. In Eq. (18), $\xi_{4,a}$ is given by

$$\xi_{4,a} = \bar{\mathcal{X}}_{4,a} - \hat{\mathcal{X}}_{4,a} \tag{20}$$

where $\bar{\mathcal{X}}_{4,a}$ is an estimate of $\mathcal{X}_{4,a}$ obtained dynamically using the cell voltage and measurement $\mathcal{X}_{5,a}$, given as follows:

$$\dot{\bar{\mathcal{X}}}_{4,a} = k_o[V_{\text{cell}} - \hat{V}_{\text{cell}} + qT_a \ln(\mathcal{X}_{5,a}) - qT_a \ln(\hat{\mathcal{X}}_{5,a})] + \bar{\eta}_{4,a}, \quad k_o > 0 \tag{21}$$

The cell voltage V_{cell} of the SOFC system is expressed as follows [20]:

$$V_{\text{cell}} = f_1(T_a, T_c, i) + \frac{R_u T_a}{nF} \ln\left(p_{\text{H}_2} p_{\text{O}_2}^{1/2} / p_{\text{H}_2\text{O}}\right) \tag{22}$$

Since $p_{\text{H}_2} = P_a \mathcal{X}_{4,a}$, $p_{\text{O}_2} = P_c \mathcal{X}_{7,c}$ and $p_{\text{H}_2\text{O}} = P_a \mathcal{X}_{5,a}$, we can express Eq. (22) as

$$V_{\text{cell}} = f_2(T_a, T_c, P_c, i, \mathcal{X}_{7,c}) + qT_a[\ln(\mathcal{X}_{4,a}) - \ln(\mathcal{X}_{5,a})] \tag{23}$$

where f_1 is the maximum electromotive force (or reversible open circuit voltage), $f_2 = f_1 + 0.5(R_u T_a/nF)\ln(P_c \mathcal{X}_{7,c})$ and $q = (R_u/nF)$ [20]. The estimate $\hat{V}_c$ is given by

$$\hat{V}_{\text{cell}} = f_2(T_a, T_c, P_c, i, \mathcal{X}_{7,c}) + qT_a[\ln(\bar{\mathcal{X}}_{4,a}) - \ln(\hat{\mathcal{X}}_{5,a})] \tag{24}$$

In Eqs. (17), (18), and (21), the terms $\eta_{1,r}$, $\eta_{1,a}$, $\eta_{2,r}$, $\eta_{2,a}$, $\eta_{3,r}$, $\eta_{3,a}$, $\eta_{4,r}$, $\eta_{4,a}$, $\bar{\eta}_{4,a}$, $\eta_{4,a}$, $\eta_{5,r}$, $\eta_{5,a}$, η_{p1}, η_{p2}, η_{p3}, and η_{p4} are included to provide upper and lower bounds on state and parameter estimates and prevent integrator wind-up. For instance, $\eta_{1,r}$ and η_{p1} are designed as

$$\eta_{1,r} = \begin{cases} -g_{1,r} & \text{if} \quad (\hat{\mathcal{X}}_{1,r} \geq 1 \text{ and } g_{1,r} > 0) \\ & \text{or} \quad (\hat{\mathcal{X}}_{1,r} \leq 0 \text{ and } g_{1,r} < 0) \\ 0 & \text{otherwise} \end{cases}$$
$$g_{1,r} = k_o \hat{\dot{N}}_o(\hat{\mathcal{X}}_{1,a} + 0.5) - \hat{\dot{N}}_{\text{in}}(\hat{\mathcal{X}}_{1,r} + 0.5) + 1.5\dot{N}_f$$

$$\eta_{p1} = \begin{cases} -g_{p1} & \text{if} \quad (\hat{\dot{N}}_{\text{in}} \geq \dot{N}_{\text{in,max}} \text{ and } g_{p1} > 0) \\ & \text{or} \quad (\hat{\dot{N}}_{\text{in}} \leq \dot{N}_{\text{in,min}} \text{ and } g_{p1} < 0) \\ 0 & \text{otherwise} \end{cases}$$
$$g_{p1} = \gamma_1 \left[(\mathcal{E}_{4,r} - \xi_{4,a})(2 - \hat{\mathcal{X}}_{4,r}) + (\mathcal{E}_{5,a} - \mathcal{E}_{5,r})(\hat{\mathcal{X}}_{5,r} + 1)\right] \tag{25, 26}$$

The upper and lower bounds on the concentration estimates are 1 and 0, respectively. The bounds on the estimates of $\hat{\dot{N}}_{in}$, $\hat{\dot{N}}_o$, $\hat{\mathcal{R}}_{2,r}$, and $\hat{\mathcal{R}}_{2,a}$ are dependent on the specific application.

5.2 Boundedness and Convergence. We first prove that $\bar{\mathcal{E}}_{4,a} = \mathcal{X}_{4,a} - \bar{\mathcal{X}}_{4,a}$ is ultimately bounded. From Eqs. (21), (23), and (24), we have

$$\dot{\bar{\mathcal{E}}}_{4,a} = -k_o q T_a[\ln(\mathcal{X}_{4,a}) - \ln(\bar{\mathcal{X}}_{4,a})] + \dot{\mathcal{X}}_{4,a} - \bar{\eta}_{4,a}$$

Taking $V = 0.5\bar{\mathcal{E}}_{4,a}^2$ as a Lyapunov function candidate and noting from the *Mean Value Theorem* that $[\ln(\mathcal{X}_{4,a}) - \ln(\bar{\mathcal{X}}_{4,a})] = \lambda \bar{\mathcal{E}}_{4,a}$, $\lambda \geq 1$, we have

$$\begin{aligned} \dot{V} &= -k_o q T_a \bar{\mathcal{E}}_{4,a}[\ln(\mathcal{X}_{4,a}) - \ln(\bar{\mathcal{X}}_{4,a})] + \bar{\mathcal{E}}_{4,a}\dot{\mathcal{X}}_{4,a} - \bar{\mathcal{E}}_{4,a}\bar{\eta}_{4,a} \\ &\leq -k_o q T_a \bar{\mathcal{E}}_{4,a}^2 + |\bar{\mathcal{E}}_{4,a}|\,|\dot{\mathcal{X}}_{4,a}| \\ &= -k_o q T_a (1-\theta_1)\bar{\mathcal{E}}_{4,a}^2 - k_o q T_a \theta_1 \bar{\mathcal{E}}_{4,a}^2 + |\bar{\mathcal{E}}_{4,a}| \sup\left(|\dot{\mathcal{X}}_{4,a}|\right) \\ &< -k_o q T_a (1-\theta_1)|\bar{\mathcal{E}}_{4,a}|^2 \\ &\quad \forall\, |\bar{\mathcal{E}}_{4,a}| > \mu_1, \quad \mu_1 \triangleq \frac{\sup\left(|\dot{\mathcal{X}}_{4,a}|\right)}{k_o q T_a \theta_1} \end{aligned} \tag{27}$$

where $0 < \theta_1 < 1$. Note that in Eq. (27), the term $\bar{\mathcal{E}}_{4,a}\bar{\eta}_{4,a} \geq 0$. This can be inferred from Eqs. (25) and (26). If $\bar{\mathcal{X}}_{4,a} \geq 1$ and $\bar{g}_{4,a} > 0$, then $\bar{\mathcal{E}}_{4,a} \leq 0$ and $\bar{\eta}_{4,a} < 0$. Similarly, if $\bar{\mathcal{X}}_{4,a} \leq 0$ and $\bar{g}_{4,a} < 0$, then $\bar{\mathcal{E}}_{4,a} \geq 0$ and $\bar{\eta}_{4,a} > 0$. Otherwise, $\bar{\eta}_{4,a} = 0$. Also note that in Eq. (27), $\sup|\dot{\mathcal{X}}_{4,a}|$ can be obtained from the range of operating conditions. It can be easily shown that $\bar{\mathcal{E}}_{4,a}$ is uniformly ultimately bounded with an ultimate bound of μ_1. Hence, by choosing k_o to be large, causing $\bar{\mathcal{X}}_{4,a}$ in Eq. (21) to be singularly perturbed, $\bar{\mathcal{E}}_{4,a}$ can be brought arbitrarily close to zero.

We next prove the ultimate boundedness of the state estimation errors $\mathcal{E}_{4,r}$, $\mathcal{E}_{4,a}$, $\mathcal{E}_{5,r}$, and $\mathcal{E}_{5,a}$. The variables $\mathcal{E}_{4,r}$, $\mathcal{E}_{5,r}$, and $\mathcal{E}_{5,a}$ are defined in Eq. (19) and

$$\mathcal{E}_{4,a} = \mathcal{X}_{4,a} - \hat{\mathcal{X}}_{4,a} \tag{28}$$

Consider the following Lyapunov function candidate:

$$V = \frac{1}{2}\left[\mathcal{E}_{4,r}^2 + \mathcal{E}_{4,a}^2 + \mathcal{E}_{5,r}^2 + \mathcal{E}_{5,a}^2 + \frac{1}{\gamma_1}\mathcal{E}_{\dot{N}_{\text{in}}}^2 + \frac{1}{\gamma_2}\mathcal{E}_{\dot{N}_o}^2 + \frac{1}{\gamma_3}\mathcal{E}_{\mathcal{R}_{2,r}}^2 + \frac{1}{\gamma_4}\mathcal{E}_{\mathcal{R}_{2,a}}^2\right]$$

where

$$\mathcal{E}_{\dot{N}_{\text{in}}} = \dot{N}_{\text{in}} - \hat{\dot{N}}_{\text{in}}, \quad \mathcal{E}_{\dot{N}_o} = \dot{N}_o - \hat{\dot{N}}_o,$$
$$\mathcal{E}_{\mathcal{R}_{2,r}} = \mathcal{R}_{2,r} - \hat{\mathcal{R}}_{2,r}, \quad \mathcal{E}_{\mathcal{R}_{2,a}} = \mathcal{R}_{2,a} - \hat{\mathcal{R}}_{2,a}$$
$$\dot{\mathcal{E}}_{\dot{N}_{\text{in}}} = -\hat{\dot{N}}_{\text{in}}, \quad \dot{\mathcal{E}}_{\dot{N}_o} = -\hat{\dot{N}}_o, \quad \dot{\mathcal{E}}_{\mathcal{R}_{2,r}} = -\hat{\dot{\mathcal{R}}}_{2,r}, \quad \dot{\mathcal{E}}_{\mathcal{R}_{2,a}} = -\hat{\dot{\mathcal{R}}}_{2,a} \tag{29}$$

From Eqs. (17), (18), (20), (28), and (29), the derivative of V along the system trajectories can be expressed as

$$\begin{aligned} \dot{V} = &-(\mathcal{L}_{4,r} + \dot{N}_{\text{in}})\mathcal{E}_{4,r}^2/N_r + (k\dot{N}_o/N_r + \dot{N}_{\text{in}}/N_a)\mathcal{E}_{4,r}\mathcal{E}_{4,a} \\ &- \dot{N}_o\mathcal{E}_{4,a}^2/N_a - (\mathcal{L}_{5,r} + \dot{N}_{\text{in}})\mathcal{E}_{5,r}^2/N_r \\ &+ (k\dot{N}_o/N_r + \dot{N}_{\text{in}}/N_a)\mathcal{E}_{5,r}\mathcal{E}_{5,a} - (\mathcal{L}_{5,a} + \dot{N}_o)\mathcal{E}_{5,a}^2/N_a \\ &+ \bar{\mathcal{E}}_{4,a}[(2 - \hat{\mathcal{X}}_{4,a})\mathcal{E}_{\dot{N}_o} + (\hat{\mathcal{X}}_{4,r} - 2)\mathcal{E}_{\dot{N}_{\text{in}}} - \mathcal{E}_{\mathcal{R}_{2,a}}]/N_a \\ &- \eta_{4,r}\mathcal{E}_{4,r} - \eta_{4,a}\mathcal{E}_{4,a} - \eta_{5,r}\mathcal{E}_{5,r} - \eta_{5,a}\mathcal{E}_{5,a} - \eta_{p1}\mathcal{E}_{\dot{N}_{\text{in}}} \\ &- \eta_{p2}\mathcal{E}_{\dot{N}_o} - \eta_{p3}\mathcal{E}_{\mathcal{R}_{2,r}} - \eta_{p4}\mathcal{E}_{\mathcal{R}_{2,a}} \end{aligned}$$

considering

$$\mathcal{E}_{4,r} = \mathcal{X}_{4,r} - \hat{\mathcal{X}}_{4,r}$$

note that $0 \leq \mathcal{X}_{4,r} \leq 1$, since $\mathcal{X}_{4,r}$ is a species mole fraction. Extending the definition in Eq. (25), $\eta_{4,r}$ is defined as

$$\eta_{4,r} = \begin{cases} -g_{4,r} & \text{if} \quad (\hat{\mathcal{X}}_{1,r} \geq 1 \text{ and } g_{4,r} > 0) \\ & \text{or} \quad (\hat{\mathcal{X}}_{4,r} \leq 0 \text{ and } g_{4,r} < 0) \\ 0 & \text{otherwise} \end{cases}$$
$$g_{4,r} = k\hat{\dot{N}}_o(\hat{\mathcal{X}}_{4,a} - 2) - \hat{\dot{N}}_{\text{in}}(\hat{\mathcal{X}}_{4,r} - 2) - 2\dot{N}_f - \hat{\mathcal{R}}_{2,r} + \mathcal{L}_{4,r}\mathcal{E}_{4,r}$$

This shows that by design $\eta_{4,r} < 0$, if $\mathcal{E}_{4,r} \leq 0$, and $\eta_{4,r} > 0$, if $\mathcal{E}_{4,r} \geq 0$, effectively setting

$$\eta_{4,r}\mathcal{E}_{4,r} \geq 0$$

The definition of η_{p1} in Eq. (26) also assures that

$$\eta_{p1}\mathcal{E}_{\dot{N}_{\text{in}}} \geq 0$$

Similarly from extensions of Eqs. (25) and (26) and the discussion after Eq. (27), it is clear that

$$\begin{gathered}\eta_{4,a}\mathcal{E}_{4,a} \geq 0, \quad \eta_{5,r}\mathcal{E}_{5,r} \geq 0, \quad \eta_{5,a}\mathcal{E}_{5,a} \geq 0 \\ \eta_{p2}\mathcal{E}_{\dot{N}_o} \geq 0, \quad \eta_{p3}\mathcal{E}_{\mathcal{R}_{2,r}} \geq 0, \quad \eta_{p4}\mathcal{E}_{\mathcal{R}_{2,a}} \geq 0\end{gathered}$$

Hence,

$$\begin{aligned}\dot{V} \leq & -\mathbf{E}_4^{\mathrm{T}}\mathbf{Q}_4\mathbf{E}_4 - \mathbf{E}_5^{\mathrm{T}}\mathbf{Q}_5\mathbf{E}_5 \\ & + \bar{\mathcal{E}}_{4,a}\left[(2-\hat{\mathcal{X}}_{4,a})\mathcal{E}_{\dot{N}_o} + (\hat{\mathcal{X}}_{4,r}-2)\mathcal{E}_{\dot{N}_{\text{in}}} - \mathcal{E}_{\mathcal{R}_{2,a}}\right]/N_a\end{aligned} \tag{30}$$

where

$$\mathbf{E}_4 = [\mathcal{E}_{4,r}\mathcal{E}_{4,a}]^{\mathrm{T}}, \quad \mathbf{E}_5 = [\mathcal{E}_{5,r}\mathcal{E}_{5,a}]^{\mathrm{T}}$$

$$\mathbf{Q}_4 = \begin{bmatrix} \dfrac{(\mathcal{L}_{4,r}+\dot{N}_{\text{in}})}{N_r} & -0.5\left(\dfrac{k\dot{N}_o}{N_r}+\dfrac{\dot{N}_{\text{in}}}{N_a}\right) \\ -0.5\left(\dfrac{k\dot{N}_o}{N_r}+\dfrac{\dot{N}_{\text{in}}}{N_a}\right) & \dfrac{\dot{N}_o}{N_a} \end{bmatrix}$$

$$\mathbf{Q}_5 = \begin{bmatrix} \dfrac{(\mathcal{L}_{5,r}+\dot{N}_{\text{in}})}{N_r} & -0.5\left(\dfrac{k\dot{N}_o}{N_r}+\dfrac{\dot{N}_{\text{in}}}{N_a}\right) \\ -0.5\left(\dfrac{k\dot{N}_o}{N_r}+\dfrac{\dot{N}_{\text{in}}}{N_a}\right) & \dfrac{(\mathcal{L}_{5,a}+\dot{N}_o)}{N_a} \end{bmatrix}$$

The molar flow rates $\dot{N}_{\text{in}}$ and $\dot{N}_o$ are positive and bounded, and $0 < k < 1$. Furthermore, in the fuel cell, $\dot{N}_o > \dot{N}_{\text{in}}$. This is because in the anode, internal steam reforming produces more product molecules from fewer reactant molecules and the electrochemical reaction conserves the number of molecules. Also, the molar contents $N_r = P_r V_r/R_u T_r$ and $N_a = P_a V_a/R_u T_a$ are positive with bounds dependent on the range of operating conditions. Hence, proper choice of the observer gains $\mathcal{L}_{4,r}$, $\mathcal{L}_{5,r}$, and $\mathcal{L}_{5,a}$ will ensure positive definiteness of $\mathbf{Q}_4$ and $\mathbf{Q}_5$. By inspection of the determinant and first principle minor of the symmetric matrix $\mathbf{Q}_4$ being positive, it is clear that the matrix is positive definite, if

$$\begin{aligned}\mathcal{L}_{4,r} &> \frac{1}{\dot{N}_o}\left[\frac{1}{4}\left(k\dot{N}_o N_a + \dot{N}_{\text{in}} N_r\right)^2 - \dot{N}_o\dot{N}_{\text{in}}\right] \\ \Rightarrow \mathcal{L}_{4,r} &\geq \left[\max(\sup(N_r), \sup(N_a))\right]^2 \sup\left(\dot{N}_o\right)\end{aligned} \tag{31}$$

Similarly, with $\mathcal{L}_{5,r} = \mathcal{L}_{5,a} = \mathcal{L}_5$, we can show that $\mathbf{Q}_5$ will be positive definite, if

$$\begin{aligned}\left(\dot{N}_{\text{in}}+\mathcal{L}_5\right)\left(\dot{N}_o+\mathcal{L}_5\right) &> \frac{1}{4}\left(k\dot{N}_o N_a + \dot{N}_{\text{in}} N_r\right)^2 \\ \Rightarrow \mathcal{L}_5 &\geq \max(\sup(N_r), \sup(N_a))\sup\left(\dot{N}_o\right)\end{aligned} \tag{32}$$

Thus, using the *Rayleigh–Ritz inequality*, we have

$$\begin{aligned}\mathbf{E}_4^{\mathrm{T}}\mathbf{Q}_4\mathbf{E}_4 &\geq \inf(\lambda_{4,\min})||\mathbf{E}_4||^2 \\ \mathbf{E}_5^{\mathrm{T}}\mathbf{Q}_5\mathbf{E}_5 &\geq \inf(\lambda_{5,\min})||\mathbf{E}_5||^2\end{aligned}$$

where $\lambda_{4,\min}$ and $\lambda_{5,\min}$ are the smaller eigenvalues of $\mathbf{Q}_4$ and $\mathbf{Q}_5$, respectively. Hence,

$$\begin{gathered}\mathbf{E}_4^T\mathbf{Q}_4\mathbf{E}_4 + \mathbf{E}_5^T\mathbf{Q}_5\mathbf{E}_5 \geq \bar{\lambda}\,||\mathbf{E}_{4,5}||^2 \\ \bar{\lambda} \triangleq \min(\inf(\lambda_{4,\min}),\ \inf(\lambda_{5,\min})), \quad \bar{\lambda} > 0\end{gathered} \tag{33}$$

where $\mathbf{E}_{4,5} = [\mathbf{E}_4\ \mathbf{E}_5]^{\mathrm{T}} = [\mathcal{E}_{4,r}\ \mathcal{E}_{4,a}\ \mathcal{E}_{5,r}\ \mathcal{E}_{5,a}]^{\mathrm{T}}$. Note that $\dot{N}_{\text{in}}$, $\dot{N}_o$, and $\mathcal{R}_{2,a}$ are bounded variables and their estimates, along with $\hat{\mathcal{X}}_{4,r}$, $\hat{\mathcal{X}}_{4,a}$, and N_a, are also bounded by design (Eqs. (17) and (18)). Therefore, from Eqs. (30) and (33), we deduce

$$\begin{aligned}\dot{V} &\leq -\bar{\lambda}\,||\mathbf{E}_{4,5}||^2 + |\bar{\mathcal{E}}_{4,a}|\,h_{\max} \\ &= -\bar{\lambda}\,(1-\theta_2)\,||\mathbf{E}_{4,5}||^2 - \bar{\lambda}\,\theta_2\,||\mathbf{E}_{4,5}||^2 + |\bar{\mathcal{E}}_{4,a}|\,h_{\max} \\ &< -\bar{\lambda}(1-\theta_2)\,||\mathbf{E}_{4,5}||^2, \\ &\qquad \forall||\mathbf{E}_{4,5}|| > \mu_2,\ \mu_2 \triangleq \sqrt{\mu_1\,h_{\max}/\bar{\lambda}\,\theta_2}\end{aligned} \tag{34}$$

where, $0 < \theta_2 < 1$ and

$$h_{\max} = \sup\left(\left[(2-\hat{\mathcal{X}}_{4,a})\mathcal{E}_{\dot{N}_o} + (\hat{\mathcal{X}}_{4,r}-2)\mathcal{E}_{\dot{N}_{\text{in}}} - \mathcal{E}_{\mathcal{R}_{2,a}}\right]/N_a\right)$$

Thus, $||\mathbf{E}_{4,5}||$ is ultimately bounded with an ultimate bound of μ_2. Furthermore, from the definitions of μ_1 and $\bar{\lambda}$ in Eqs. (27) and (33), we infer that μ_2 can be made arbitrarily small by choosing large observer gains k_o and $\bar{\lambda}$.

Next, we show that $\hat{\dot{N}}_{in}$, $\hat{\dot{N}}_o$, $\hat{\mathcal{R}}_{2,r}$, and $\hat{\mathcal{R}}_{2,a}$ converge to their true values with small bounded errors. Since μ_2 can be made arbitrarily small, for every $t_0 \geq 0$, there exists $T \geq 0$ such that $\eta_{4,r} = \eta_{4,a} = \eta_{5,r} = \eta_{5,a} = 0$ for $t > t_0 + T$. Therefore, for sufficiently large t_0, the state equation for $\mathbf{E}_{4,5}$ can be written as

$$\dot{\mathbf{E}}_{4,5} = \mathbf{A}_{4,5}\,\mathbf{E}_{4,5} + \mathbf{B}_{4,5}\,\mathbf{E}_p \tag{35}$$

where $\mathbf{E}_p = [\mathcal{E}_{\dot{N}_{in}}\ \mathcal{E}_{\dot{N}_o}\ \mathcal{E}_{\mathcal{R}_{2,r}}\ \mathcal{E}_{\mathcal{R}_{2,a}}]^{\mathrm{T}}$

$$\mathbf{A}_{4,5} = \begin{bmatrix} -\dfrac{(\mathcal{L}_{4,r}+\dot{N}_{\text{in}})}{N_r} & \dfrac{k\dot{N}_o}{Nr} & 0 & 0 \\ \dfrac{\dot{N}_{\text{in}}}{N_a} & -\dfrac{\dot{N}_o}{N_a} & 0 & 0 \\ 0 & 0 & -\dfrac{(\mathcal{L}_{5,r}+\dot{N}_{\text{in}})}{N_r} & \dfrac{k\dot{N}_o}{Nr} \\ 0 & 0 & \dfrac{\dot{N}_{\text{in}}}{N_a} & -\dfrac{(\mathcal{L}_{5,r}+\dot{N}_o)}{N_a} \end{bmatrix}$$

$$\mathbf{B}_{4,5} = \begin{bmatrix} -\dfrac{\left(\hat{\mathcal{X}}_{4,r}-2\right)}{N_r} & \dfrac{k\left(\hat{\mathcal{X}}_{4,a}-2\right)}{N_r} & -\dfrac{1}{N_r} & 0 \\ \dfrac{\left(\hat{\mathcal{X}}_{4,r}-2\right)}{N_a} & -\dfrac{\left(\hat{\mathcal{X}}_{4,a}-2\right)}{N_a} & 0 & -\dfrac{1}{N_a} \\ -\dfrac{\left(1+\hat{\mathcal{X}}_{5,r}\right)}{N_r} & \dfrac{k\left(1+\hat{\mathcal{X}}_{5,a}\right)}{N_r} & \dfrac{1}{N_r} & 0 \\ \dfrac{\left(1+\hat{\mathcal{X}}_{5,r}\right)}{N_a} & -\dfrac{\left(1+\hat{\mathcal{X}}_{5,a}\right)}{N_a} & 0 & \dfrac{1}{N_a} \end{bmatrix} \tag{36}$$

From Eq. (35), we have

$$\ddot{\mathbf{E}}_{4,5} = \mathbf{A}_{4,5}\,\dot{\mathbf{E}}_{4,5} + \dot{\mathbf{A}}_{4,5}\,\mathbf{E}_{4,5} + \dot{\mathbf{B}}_{4,5}\,\mathbf{E}_p + \mathbf{B}_{4,5}\,\dot{\mathbf{E}}_p \tag{37}$$

In Eq. (37), $||\mathbf{A}_{4,5}||$ and $||\dot{\mathbf{A}}_{4,5}||$ are bounded with bounds on N_r, N_a, $\dot{N}_r$, $\dot{N}_a$, $\dot{N}_{\text{in}}$, $\dot{N}_o$, $\ddot{N}_{\text{in}}$, and $\ddot{N}_o$ governed by the operating conditions of the fuel cell. $||\mathbf{E}_{4,5}||$ was shown to be bounded with an ultimate bound of μ_2. $||\mathbf{B}_{4,5}||$ and $||\dot{\mathbf{B}}_{4,5}||$ are bounded due to the observer design in Eq. (17). $||\mathbf{E}_p||$ and $||\dot{\mathbf{E}}_p||$ are also bounded by

virtue of the design of the adaptation laws in Eq. (18). Finally, $\|\dot{\mathbf{E}}_{4,5}\|$ is bounded as inferred from Eq. (35) and the foregoing discussion. Hence, $\|\ddot{\mathbf{E}}_{4,5}\|$ is bounded, and

$$\|\mathbf{E}_{4,5}\| \le \mu_2,\ \|\ddot{\mathbf{E}}_{4,5}\| \le \mu_3,\ \mu_2,\ \mu_3 > 0 \Rightarrow \|\dot{\mathbf{E}}_{4,5}\| \le 2\sqrt{\mu_2\,\mu_3} \tag{38}$$

The following lemma is presented to justify the above statement:

LEMMA 1. *Let a function and its time derivatives be f(t), $\dot{f}(t)$, and $\ddot{f}(t)$, respectively, and all three functions be bounded as follows:* $\sup_{\forall t}|f(t)| = \mu_2$, $\sup_{\forall t}|\dot{f}(t)| = \mu$, *and* $\sup_{\forall t}|\ddot{f}(t)| = \mu_3$. *Then,* $\mu \le 2\sqrt{\mu_2\mu_3}$.

Proof. Without loss of generality, we can say

$$\frac{df}{\dot{f}} = \frac{d\dot{f}}{\ddot{f}} \Rightarrow \ddot{f}\,df = \dot{f}\,d\dot{f}$$

Integrating both sides, we get

$$\int_{\dot{f}_0}^{\dot{f}} \dot{f}\,d\dot{f} = \int_{f_0}^{f} \ddot{f}\,df \Rightarrow \frac{1}{2}\left(\dot{f}^2 - \dot{f}_0^2\right) = \int_{f_0}^{f} \ddot{f}\,df$$

Since $|\ddot{f}| \le \mu_3$ and from the successive use of inequalities, we have

$$\int_{f_0}^{f} \ddot{f}\,df \le \left|\int_{f_0}^{f} \ddot{f}\,df\right| \le \left|\int_{f_0}^{f} |\ddot{f}|\,df\right| \le \left|\mu_3 \int_{f_0}^{f} df\right| = \mu_3\left|\int_{f_0}^{f} df\right| = \mu_3|f - f_0|$$

Next, from the upper bound of f

$$|f - f_0| \le |f| + |f_0| = 2\mu_2$$
$$\Rightarrow \frac{1}{2}\left(\dot{f}^2 - \dot{f}_0^2\right) \le 2\mu_3\mu_2$$

Finally, the maximum value of $1/2(\dot{f}^2 - \dot{f}_0^2)$ is $1/2(\mu^2 - 0) = \mu^2/2$. Thus, $\mu \le 2\sqrt{\mu_2\mu_3}$ □

From Eqs. (35) and (37), we deduce that

$$\|\ddot{\mathbf{E}}_{4,5}\| \le c_1\,\mu_2 + c_2, \quad \Rightarrow \quad \mu_3 = c_1\mu_2 + c_2 \tag{39}$$

where c_1 and c_2 are fixed positive constants given by

$$c_1 = \sup(\|\mathbf{A}_{4,5}\|^2 + \|\dot{\mathbf{A}}_{4,5}\|),$$
$$c_2 = \sup([\|\mathbf{A}_{4,5}\|\,\|\mathbf{B}_{4,5}\|\|\dot{\mathbf{B}}_{4,5}\|]\|\mathbf{E}_p\|\|\mathbf{B}_{4,5}\|\,\|\dot{\mathbf{E}}_p\|)$$

From Eqs. (38) and (39), we conclude that as $\mu_2 \to 0$ with large values of the observer gains k_o and $\bar{\lambda}$, both $\|\mathbf{E}_{4,5}\|$ and $\|\dot{\mathbf{E}}_{4,5}\|$ approach ultimate bounds that are arbitrarily close to zero. From Eq. (36), we infer that since $\|\mathbf{E}_{4,5}\| \le \mu_2$, for all feasible operating conditions of the SOFC, $\mathbf{B}_{4,5}$ will be nonsingular, and therefore, from Eq. (35), we have

$$\mathbf{E}_p = \mathbf{B}_{4,5}^{-1}[\dot{\mathbf{E}}_{4,5} - \mathbf{A}_{4,5}\,\mathbf{E}_{4,5}]$$
$$\Rightarrow \|\mathbf{E}_p\| \le \|\mathbf{B}_{4,5}^{-1}\|\,[2\sqrt{\mu_2\,(c_1\,\mu_2 + c_2)} + \|\mathbf{A}_{4,5}\|\,\mu_2] \tag{40}$$

From Eq. (40), it is clear that as $\mu_2 \to 0$ so will $\|\mathbf{E}_p\|$ and this implies convergence of $\hat{\dot{N}}_{\text{in}}$, $\hat{\dot{N}}_o$, $\hat{\mathcal{R}}_{2,r}$, and $\hat{\mathcal{R}}_{2,a}$ to their true values with small bounded errors.

Finally, we show that the remaining state estimates, $\hat{\mathcal{X}}_{1,r}$, $\hat{\mathcal{X}}_{2,r}$, $\hat{\mathcal{X}}_{3,r}$, $\hat{\mathcal{X}}_{1,a}$, $\hat{\mathcal{X}}_{2,a}$, and $\hat{\mathcal{X}}_{3,a}$, are ultimately bounded around their true values with small errors. We prove this by establishing the *input-to-state stability* (ISS) property [21] of $\mathcal{E}_{1,r}$, $\mathcal{E}_{1,a}$, $\mathcal{E}_{2,r}$, $\mathcal{E}_{2,a}$, $\mathcal{E}_{3,r}$, and $\mathcal{E}_{3,a}$, where

$$\mathcal{E}_{1,r} = \mathcal{X}_{1,r} - \hat{\mathcal{X}}_{1,r}, \quad \mathcal{E}_{1,a} = \mathcal{X}_{1,a} - \hat{\mathcal{X}}_{1,a}$$
$$\mathcal{E}_{2,r} = \mathcal{X}_{2,r} - \hat{\mathcal{X}}_{2,r}, \quad \mathcal{E}_{2,a} = \mathcal{X}_{2,a} - \hat{\mathcal{X}}_{2,a}$$
$$\mathcal{E}_{3,r} = \mathcal{X}_{3,r} - \hat{\mathcal{X}}_{3,r}, \quad \mathcal{E}_{3,a} = \mathcal{X}_{3,a} - \hat{\mathcal{X}}_{3,a}$$

Consider the state equation of $\mathbf{E}_3$, which is given as

$$\dot{\mathbf{E}}_3 = \mathbf{Q}_3\,\mathbf{E}_3 + \mathbf{B}_3\,\mathbf{E}_p \tag{41}$$

where

$$\mathbf{E}_3 = [\mathcal{E}_{3,r}\mathcal{E}_{3,a}]^{\mathrm{T}}, \quad \mathbf{Q}_3 = \begin{bmatrix} \frac{\dot{N}_{\text{in}}}{N_r} & -\frac{k\dot{N}_o}{N_r} \\ -\frac{\dot{N}_{\text{in}}}{N_a} & \frac{\dot{N}_o}{N_a} \end{bmatrix} \tag{42}$$

and

$$\mathbf{B}_3 = \begin{bmatrix} -\frac{\left(\hat{\mathcal{X}}_{3,r} - 0.5\right)}{N_r} & \frac{k\left(\hat{\mathcal{X}}_{3,a} - 0.5\right)}{N_r} & -\frac{1}{N_r} & 0 \\ \frac{\left(\hat{\mathcal{X}}_{3,r} - 0.5\right)}{N_a} & -\frac{\left(\hat{\mathcal{X}}_{3,a} - 0.5\right)}{N_a} & 0 & -\frac{1}{N_a} \end{bmatrix}$$

Considering $\mathbf{B}_3\,\mathbf{E}_p$ to be the input in Eq. (41), the origin of the unforced system

$$\dot{\mathbf{E}}_3 = \mathbf{Q}_3\,\mathbf{E}_3$$

is globally exponentially stable since $\mathbf{Q}_3$ and $\dot{\mathbf{Q}}_3$ are bounded, and the pointwise eigenvalues of $\mathbf{Q}_3$ are negative and real [22]. Hence, the system in Eq. (41) is ISS. Therefore, $\|\mathbf{E}_3\|$ is ultimately bounded by a class $\mathcal{K}$ function of $\sup(\|\mathbf{B}_3\|)\sup(\|\mathbf{E}_p\|)$. From Eq. (40), it is clear that as $\mu_2 \to 0$ so will $\|\mathbf{E}_p\|$. Thus, as $\|\mathbf{E}_p\| \to 0$ so will $\|\mathbf{E}_3\|$, confirming that the convergence of $\hat{\dot{N}}_{\text{in}}$, $\hat{\dot{N}}_o$, $\hat{\mathcal{R}}_{2,r}$, and $\hat{\mathcal{R}}_{2,a}$ to their true values will lead to correct estimation of $\mathcal{X}_{3,r}$ and $\mathcal{X}_{3,a}$. Similar conclusions can be drawn for $\mathcal{X}_{1,r}$, $\mathcal{X}_{2,a}$, $\mathcal{X}_{2,r}$, and $\mathcal{X}_{2,a}$ by performing similar analysis as above for the state equations of $\mathbf{E}_1 = [\mathcal{E}_{1,r}\mathcal{E}_{1,a}]^{\mathrm{T}}$ and $\mathbf{E}_2 = [\mathcal{E}_{2,r}\mathcal{E}_{2,a}]^{\mathrm{T}}$.

5.3 Simulations. We provide simulation results to demonstrate the performance of the voltage-based observer design presented in Secs. 4 and 5.

The observer was tested on the comprehensive fuel cell model that captures the details of heat and mass transfer, chemical kinetics, and electrochemistry. We performed an open-loop simulation of the plant model in conjunction with the observer. For the simulation, we chose $\dot{N}_f = 0.01$ mol/s, $\dot{N}_{\text{air}} = 0.1$ mol/s, and $k = 0.75$. The current demand was changed in steps as given below:

$$i = \begin{cases} 65 & \text{for} \quad 0 \le t \le 60 \\ 70 & \text{for} \quad 60 < t \le 110 \\ 68 & \text{for} \quad 110 < t \end{cases}$$

The values of the observer gains are chosen as $k_o = 10$, $\mathcal{L}_{4,r} = \mathcal{L}_5 = 1$, and $\gamma_1 = \gamma_2 = \gamma_3 = \gamma_4 = 250$. The estimation algorithm was switched on at $t = 10$ s and was left active for the rest of the simulation. The estimates $\hat{\dot{N}}_{\text{in}}$, $\hat{\dot{N}}_o$, $\hat{\mathcal{R}}_{2,r}$, and $\hat{\mathcal{R}}_{2,a}$ along with their model-generated actual values are plotted in Fig. 4. The accuracy of these estimates is important, since it directly

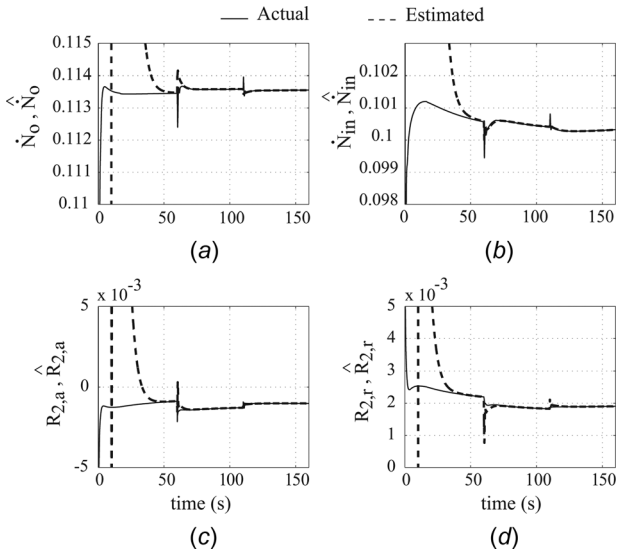

Fig. 4 $\dot{N}_{\text{in}}$, $\dot{N}_o$, $\mathcal{R}_{2,r}$, and $\mathcal{R}_{2,a}$ and their estimates

determines the estimation accuracy of CH_4, CO, and CO_2 concentrations, which are shown in Fig. 5. The corresponding plots of H_2 and H_2O are omitted for conciseness.

We have outlined an observer design procedure that uses three concentration sensors and cell voltage measurement. The number of concentration sensors can be further reduced by one, if measurements of the net molar flow rates at the exit of the reformer and anode, i.e., if $\dot{N}_{\text{in}}$ and $\dot{N}_o$, are available. The development of the observer equations is left to the reader for the sake of brevity.

6 Reduced Order Observer for Estimation of Fuel Utilization U

Dynamic load following limitations of the fuel cell for SOFCs are attributed to the fuel delivery systems of SOFCs and its slower

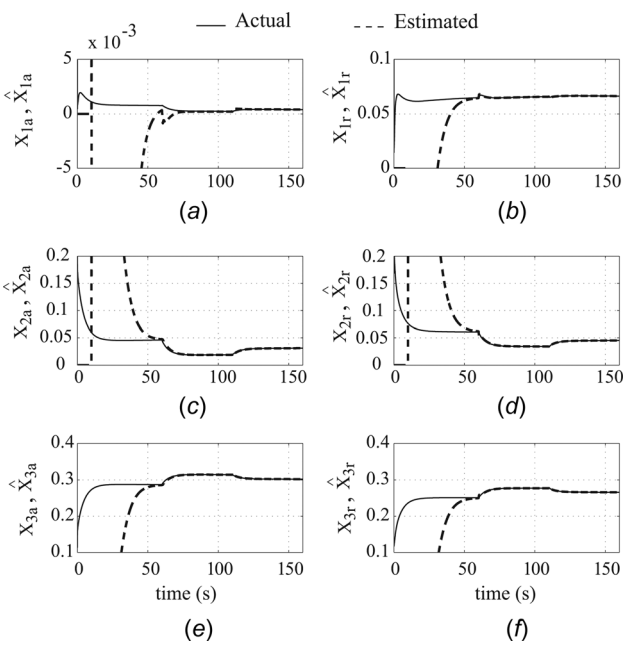

Fig. 5 CH_4, CO, and CO_2 mole fractions and their estimates

mechanical subsystems, such as pumps, valves, and reformers (reference snyder). As a result, hydrogen starvation can occur potentially resulting in voltage drop, anode oxidation, and catalyst corrosion [1]. These limitations are reflected in the transient response of a single performance variable, which is fuel utilization, often characterized by the variable U. Thus, for optimal performance U must be maintained around an optimal value (typically 80–90%) even under significant power fluctuations [23]. Thus, further extending the above observer, the ensuing discussion proposes a reduced order observer for estimation of U. The aim of using such an observer is to achieve better transient control to avoid aforementioned limitations of SOFCs.

For the considered SOFC configuration, fuel utilization is mathematically defined as follows [1,6]:

$$U = 1 - [\dot{N}_o(4\mathcal{X}_{1,a} + \mathcal{X}_{2,a} + \mathcal{X}_{4,a})]/[\dot{N}_{\text{in}}(4\mathcal{X}_{1,r} + \mathcal{X}_{2,r} + \mathcal{X}_{4,r})]$$
$$\Rightarrow \quad U = 1 - \dot{N}_o\zeta_a/\dot{N}_{\text{in}}\zeta_r \tag{43}$$

Based on Eq. (3) which shows that the maximum H_2 from CH_4 and CO are 4 and 1, respectively, it can be seen from the mass-balance Eqs. (7) and (13) that by defining two variables ζ_r and ζ_a as

$$\begin{aligned}\zeta_r &= 4\mathcal{X}_{1,r} + \mathcal{X}_{2,r} + \mathcal{X}_{4,r}\\ \zeta_a &= 4\mathcal{X}_{1,a} + \mathcal{X}_{2,a} + \mathcal{X}_{4,a}\end{aligned} \tag{44}$$

a state transformation can be used. As a result, the reaction rates in the aforementioned equations do not appear when considering the potential utilization of H_2. From Eqs. (7), (11), (13), and (43) at steady-state, we have

$$\begin{aligned}\frac{d}{dt}(N_r\zeta_r) &= k\dot{N}_o\zeta_a - \dot{N}_{\text{in}}\zeta_r + 4\dot{N}_f\\ \frac{d}{dt}(N_a\zeta_a) &= -\dot{N}_o\zeta_a + \dot{N}_{\text{in}}\zeta_r + i\mathcal{N}_{\text{cell}}/nF\end{aligned} \tag{45}$$

It should be noted that the ζ_r and ζ_a indicate maximum potential H_2 production during system reactions, which is conserved [24].

In the existing method for transient control, the current regulation (CR) is based on the measurement $\dot{N}_f$ that occurs upstream of the reformer [25]. Hence, while incorporating the delay due to fuel supply system, the delay introduced by the reformer is not incorporated by the CR. To incorporate the effect of the delay from the reformer, a nonlinear observer for the SOFC system is proposed as follows:

$$\begin{aligned}N_r\dot{\hat{\zeta}}_r &= k\dot{N}_o\hat{\zeta}_a - \dot{N}_{\text{in}}\hat{\zeta}_r + 4\dot{N}_f\\ N_a\dot{\hat{\zeta}}_a &= -\dot{N}_o\hat{\zeta}_a + \dot{N}_{\text{in}}\hat{\zeta}_r + i\mathcal{N}_{\text{cell}}/nF\end{aligned} \tag{46}$$

Note that due to the specific definition of ζ_r and ζ_a, their dynamic equations, Eq. (45), and hence the observer equations Eq. (46) are independent of the internal reaction rates. This implies that while observer-based species concentration estimation would require concentration sensors, estimating ζ_r and ζ_a would not. This is exploited in developing the reduced order observer.

Note that $\dot{N}_f$ is measured, i is an input, and $\mathcal{N}_{\text{cell}}$, n, and F are known constants. In addition, for implementing this observer, we assume that the measurements of the bulk flow rates $\dot{N}_{\text{in}}$ and $\dot{N}_o$ are available, and the average temperature and pressure of the reformer and the anode are available. In this preliminary study, the effect of measurement errors is not incorporated but will be considered in future work. The equation for the error variables $E_r = \zeta_r - \hat{\zeta}_r$ and $E_a = \zeta_a - \hat{\zeta}_a$ are

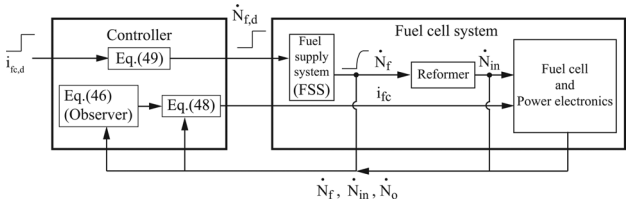

Fig. 6 Observer-based approach for transient utilization control

$$\dot{\mathbf{E}} = -A(t)\mathbf{E} + \Delta(t)$$
$$\mathbf{E} = [E_r \; E_a]^{\mathrm{T}}, \quad A(t) = \begin{bmatrix} \frac{\dot{N}_{\mathrm{in}}}{N_r} & -k\frac{\dot{N}_o}{N_r} \\ -\frac{\dot{N}_{\mathrm{in}}}{N_a} & \frac{\dot{N}_o}{N_a} \end{bmatrix}, \tag{47}$$
$$\Delta = \begin{bmatrix} -\frac{\dot{N}_r\zeta_r}{N_r} - \frac{\dot{N}_a\zeta_a}{N_a} \end{bmatrix}^{\mathrm{T}}$$

Considering $\Delta(t)$ to be the input in Eq. (47), the origin of the unforced system $\dot{\mathbf{E}} = -A(t)\mathbf{E}$ is globally exponentially stable since due to finite operating conditions, $A(t)$ and $\dot{A}(t)$ are bounded and the pointwise eigenvalues of $A(t)$ are negative and real, Ref. [22]. Hence, the system in Eq. (47) is ISS, Ref. [21]. Therefore, $||\mathbf{E}||$ is ultimately bounded by a class $\mathcal{K}$ function of $\sup(||\Delta(t)||)$. Thus, as $||\Delta(t)|| \to 0$ so will $||\mathbf{E}||$, confirming ultimate boundedness property of $||\mathbf{E}||$. This shows that the proposed observer will provide bounded estimate of ζ_r with the estimation error dependent on the magnitude of $\Delta(t)$. At steady-state, $\hat{\zeta}_r$ will provide the correct estimate.

Then, from Eqs. (43) and (45), and noting that the measurement of $\dot{N}_{\mathrm{in}}$ and the estimate $\hat{\zeta}_r$ are available, the CR method can be modified as follows:

$$U_{\mathrm{ss}} = i\mathcal{N}_{\mathrm{cell}}/nF\dot{N}_{\mathrm{in}}\zeta_r \Rightarrow i = U_{\mathrm{ss}}nF\dot{N}_{\mathrm{in}}\hat{\zeta}_r/\mathcal{N}_{\mathrm{cell}} \tag{48}$$

with $\dot{N}_{f,d}$ calculated based on the demanded $i_{f_{c,d}}$, according to (see Ref. [25])

$$\dot{N}_{f,d} = i_{f_{c,d}}N_{\mathrm{cell}}[1-(1-U_{\mathrm{ss}})k]/4nFU_{\mathrm{ss}} \tag{49}$$

6.1 Simulations. The SOFC system is simulated with target $U_{\mathrm{ss}} = 85\%$, $i = 10$ A for $t < 150$ s, and 20, 30, 50 A for $t \geq 150$ s. For each step change in i, we compare the two approaches, based on steady-state invariant property [25] and the observer-based approach outlined in Fig. 6. The simulation results are provided in Fig. 7. Note that Figs. 7(*a*), 7(*d*), and 7(*g*) correspond to step change to 20 A, plots (*b*), (*e*), and (*h*) correspond to step change to 30 A, and plots (*c*), (*f*), and (*i*) correspond to step change to 50 A.

In Figs. 7(*a*)–7(*c*), we compare the transient utilization obtained by the two methods. Note that the observer-based method provides better transient attenuation and its effectiveness is more pronounced for larger power fluctuations. The $\hat{\zeta}$ estimation by the observer is depicted for the three-step changes in plots (*d*)–(*f*). The transient discrepancies are attributed to $\Delta(t)$, given in Eq. (47). CR through the observer-based approach is compared to the existing approach in plots (*g*)–(*i*). It is evident from Fig. 7 that the observer-based approach provides better transient utilization control over the existing approach.

We next observe that if the delay D2, which is due to the reformer dynamics, is significantly higher than delay D1 induced by the FSS, then the observer based approach may provide a greater benefit. To test this, we artificially increased the reformer

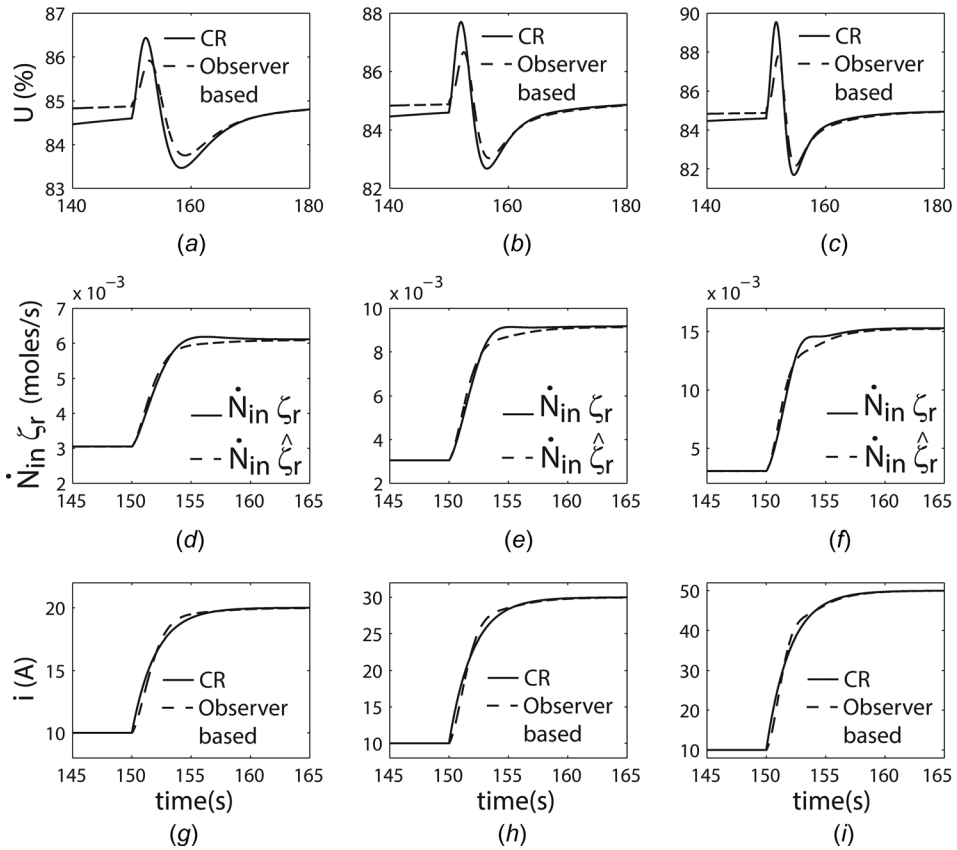

Fig. 7 Simulation results for observer-based approach for transient utilization control

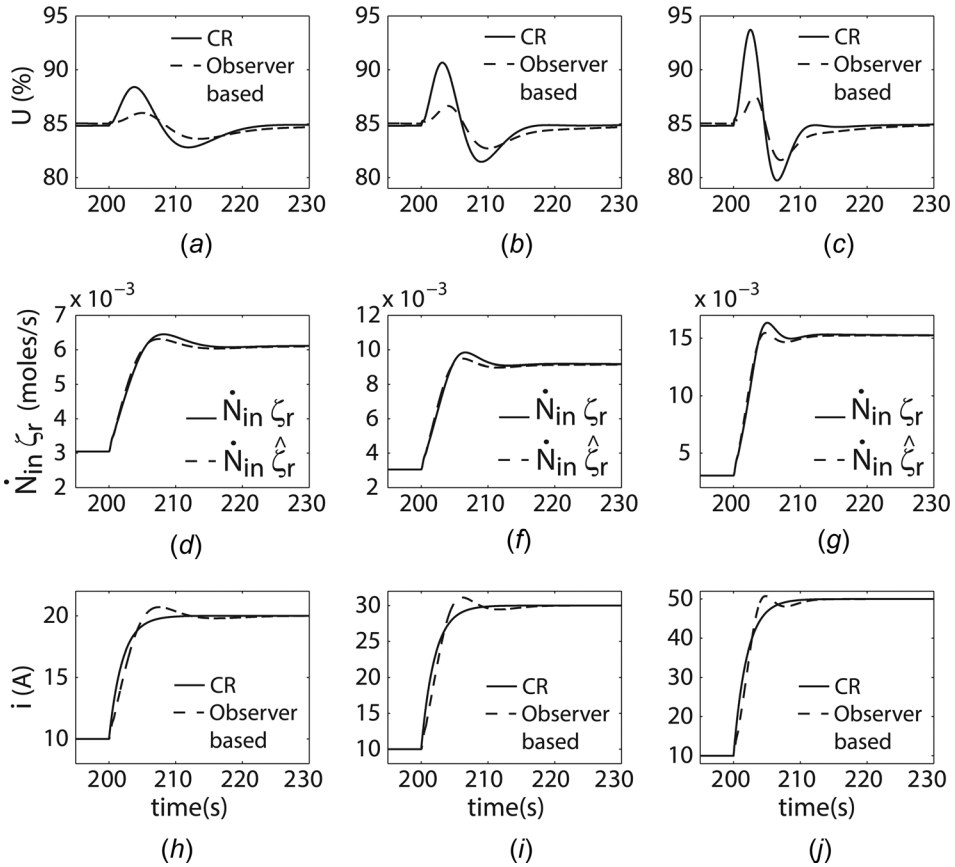

Fig. 8 Simulation results for observer-based approach for transient utilization control with increased reformer volume

volume in the system considered above by a factor of 4. Increasing the reformer volume could lead to slower reformer dynamics if the operating conditions are similar as before, and thereby increase D2. In the above simulation, the volume of the steam reformer is 6×10^{-4} m^3. We increase the steam reformer volume to 2.4×10^{-3} m^3 and rerun the simulations shown in Fig. 7. The simulation results with increased reformer volume are given in Fig. 8. As in the previous simulation, Figs. 8(*a*), 8(*d*), and 8(*g*) correspond to step change in i from 10 A to 20 A, plots (*b*), (*e*), and (*h*) correspond to step change to 30 A, and plots (*c*), (*f*), and (*i*) correspond to step change to 50 A. As expected, the observer-based CR approach provides significantly higher transient attenuation in comparison to the existing CR approach, as evident from Figs. 8(*a*) to 8(*c*).

7 Conclusion

We have presented an observer design for species concentration estimation in recirculation-based SOFC systems. In this design, we do not assume the knowledge of the rates of reforming reactions. Instead, they are treated as variables that are dynamically estimated in conjunction with dynamic concentration estimation. The proposed observer design is based on cell voltage measurement. We show that this observer guarantees ultimate boundedness of state and parameter estimation errors. The error bounds can made small through proper choice of observer gains. Simulation results are provided in support of our design. A reduced order observer for estimation of fuel utilization has also been presented. The observer estimates effective available hydrogen at the anode inlet. It uses total flow measurement rather than using sensors for individual species. The fuel cell current is regulated by combining the observed utilization with a steady-state relation. This approach provides improved transient control of U over an invariant property-based method, previously developed. In comparison to the original CR approach, the observer has increased sensing requirement but does not require a knowledge of the internal reaction rates. It is, however, found to be more effective for slow reforming processes.

Acknowledgment

Part of this work was supported by NSF Grant No. 1158845 and the Office of Naval Research Grant No. N000140910272.

Nomenclature

F = Faraday's constant, 96,485.34 C/mol
i = current draw, A
k = anode recirculation fraction
n = number of electrons participating in electrochemical reaction, (= 2)
N = number of moles, mol
$\dot{N}_f$ = molar flow rate of fuel, mol/s
$\dot{N}_o$ = anode exit flow rate, mol/s
$\dot{N}_{\text{air}}$ = molar flow rate of air, mol/s
$\dot{N}_{\text{in}}$ = anode inlet flow rate, mol/s
r_e = rate of electrochemical reaction, mol/s
$r_{\text{I}}, r_{\text{II}}, r_{\text{III}}$ = rates of reforming reactions, mol/s
R_u = universal gas constant, 8.314 J/mol K
V_{cell} = cell voltage, V
$\mathcal{N}_{\text{cell}}$ = number of cells
ζ = molar flow rate, mol/s
$\mathcal{R}$ = species rate of formation, mol/s
$\mathcal{X}$ = species mole fraction

Subscripts

a = anode control volume
ex = exit condition of control volume

g = generic gas control volume
i, j = values of 1–7 represent species CH_4, CO, CO_2, H_2, H_2O, N_2, and O_2
in = inlet condition of control volume
r = reformate control volume
s = solid volume
ss = steady-state

References

[1] Mueller, F., Brouwer, J., Jabbari, F., and Samuelsen, S., 2006, "Dynamic Simulation of an Integrated Solid Oxide Fuel Cell System Including Current-Based Fuel Flow Control," ASME J. Fuel Cell Sci. Technol., **3**(2), pp. 144–154.

[2] Ferrari, M. L., Traverso, A., Magistri, L., and Massardo, A. F., 2005, "Influence of Anodic Recirculation Transient Behavior on the SOFC Hybrid System Performance," J. Power Sources, **149**, pp. 22–32.

[3] Kandepu, R., Imsland, L., Foss, B. A., Stiller, C., Thorud, B., and Bolland, O., 2007, "Modeling and Control of a SOFC-GT-Based Autonomous Power System," Energy, **32**(4), pp. 406–417.

[4] Xu, J., and Froment, G. F., 1989, "Methane Steam Reforming, Methanation and Water-Gas Shift: I. Intrinsic Kinetics," AIChE J., **35**(1), pp. 88–96.

[5] Hall, D. J., and Colclaser, R. G., 1999, "Transient Modeling and Simulation of a Tubular Solid Oxide Fuel Cell," IEEE Trans. Energy Convers., **14**(3), pp. 749–753.

[6] Lazzaretto, A., Toffolo, A., and Zanon, F., 2004, "Parameter Setting for a Tubular SOFC Simulation Model," ASME J. Energy Resour. Technol., **126**(1), pp. 40–46.

[7] Li, P., and Chyu, M. K., 2003, "Simulation of the Chemical/Electrochemical Reactions and Heat/Mass Transfer for a Tubular SOFC in a Stack," J. Power Sources, **124**(2), pp. 487–498.

[8] Xue, X., Tang, J., Sammes, N., and Du, Y., 2005, "Dynamic Modeling of Single Tubular SOFC Combining Heat/Mass Transfer and Electrochemical Reaction Effects," J. Power Sources, **142**(1–2), pp. 211–222.

[9] Xi, H., Sun, J., and Tsourapas, V., 2007, "A Control Oriented Low Order Dynamic Model for Planar SOFC Using Minimum Gibbs Free Energy Method," J. Power Sources, **165**(1), pp. 253–266.

[10] Arcak, M., Gorgun, H., Pedersen, L. M., and Varigonda, S., 2004, "A Nonlinear Observer Design for Fuel Cell Hydrogen Estimation," IEEE Trans. Control Syst. Technol., **12**(1), pp. 101–110.

[11] Bastin, G., and Dochain, D., 1990, *On-Line Estimation and Adaptive Control of Bioreactors*, Elsevier Science Publishers, Amsterdam, The Netherlands.

[12] Gorgun, H., Arcak, M., Varigonda, S., and Bortoff, S. A., 2005, "Observer Designs for Fuel Processing Reactors in Fuel Cell Power Systems," Int. J. Hydrogen Energy, **30**(4), pp. 447–457.

[13] Iyer, N. M., and Farell, A. E., 1996, "Design of a Stable Adaptive Nonlinear Observer for an Exothermic Stirred Tank Reactor," Comput. Chem. Eng., **20**(9), pp. 1141–1147.

[14] Soroush, M., 1997, "Nonlinear State-Observer Design With Application to Reactors," Chem. Eng. Sci., **52**(3), pp. 387–404.

[15] Dochain, D., 2003, "State Observers for Processes With Uncertain Kinetics," Int. J. Control, **76**(15), pp. 1483–1492.

[16] Das, T., Narayan, S., and Mukherjee, R., 2010, "Steady-State and Transient Analysis of a Steam Reformer Based Solid Oxide Fuel Cell System," ASME J. Fuel Cell Sci. Technol., **7**, pp. 1–10.

[17] Incropera, F. P., and DeWitt, D. P., 2002, *Fundamentals of Heat and Mass Transfer*, 5th ed., Wiley, New York.

[18] Bove, R., Lunghi, P., and Sammes, N. M., 2005, "SOFC Mathematic Model for Systems Simulations—Part 2: Definition of an Analytical Model," Int. J. Hydrogen Energy, **30**(2), pp. 189–200.

[19] Das, T., and Mukherjee, R., 2007, "Observer Design for a Steam Reformer Based Solid Oxide Fuel Cell System With Anode Recirculation," ASME Paper No. IMECE2007-42332.

[20] Larminie, J., and Dicks, A., 2003, *Fuel Cell Systems Explained*, 2nd ed., Wiley, New York.

[21] Khalil, H. K., 2002, *Nonlinear Systems*, 3rd ed., Prentice Hall, Upper Saddle River, NJ.

[22] Rugh, W. J., 1996, *Linear Systems Theory*, 2nd ed., Prentice Hall, Upper Saddle River, NJ.

[23] Huang, K., and Goodenough, J. B., 2009, *Solid Oxide Fuel Cell Technology*, 1st ed., Woodhead Publishing, Cambridge, UK.

[24] Aris, R., 1989, *Elementary Chemical Reactor Analysis*, Butterworth Publishers, Stoneham, NY.

[25] Das, T., and Slippey, A., 2010, "Observer Based Transient Fuel Utilization Control for Solid Oxide Fuel Cells," ASME No. DSCC2010-4182.